Zippered Shear Zone Model for Interacting Shear Zones in the Borborema Province, Brazil, as Constrained by U-Pb Dating

Carlos F. Ávila[1] [iD], **Carlos J. Archanjo[1]**, **Haakon Fossen[2]** [iD], **and Maria Helena B. M. Hollanda[1]**

[1]Instituto de Geociências, Universidade de São Paulo, São Paulo, Brazil, [2]Museum of Natural History and Department of Earth Sciences, University of Bergen, Bergen, Norway

Abstract Shear zones typically interact to form connected systems or networks to accommodate crustal deformation, but our knowledge of how this happens is fragmentary. Understanding branching and interacting shear zones requires knowledge of timing, deformation kinematics, and rheology. The Senador Pompeu, Tauá, and Cococi strike-slip shear zones of the Borborema Province (NE Brazil) have a central role and location in the Neoproterozoic assembly of Gondwana and provide a means to understand shear zone interaction. We apply (i) U-Pb in situ SHRIMP analysis of zircons from syntectonic plutons and dykes to constrain the timing of shearing and (ii) vorticity and strain analysis on pluton's megacrystic facies deformed in the magmatic state and during final stages of crystallization. Obtained ages show that the shear zone pair was active under high temperature at 583.5 ± 4.6 Ma, while felsic dykes were emplaced in the brittle regime in the wall rocks. Average vorticity estimates of 0.70 indicate a strong component of pure shear in the shear zones. Despite the transpressional character, the dispersion in estimates of thinning and thickening for the Senador Pompeu shear zone highlights variations of offset rate for the interacting branches that leads to localized transtension. We conclude that the kinematic framework of the Senador Pompeu and Tauá conjugate pair involves the formation of a dextrally closing zipper structure involving the trailing Cococi shear zone to the southwest, which in turn caused the northeastward extrusion of the enclosed crustal wedge and possibly activation of the nappe system of the Ceará Central domain.

1. Introduction

Continental-scale shear zones are a most fundamental tectonic feature of orogenic deformation. As such they have been subject to extensive structural and geodynamic investigations and found to play a key role in crustal deformation and in accompanying lithospheric extrusion (Daout et al., 2018; Yakovlev & Clark, 2014). Heterogeneities of shear zones and faults have also been largely regarded as properties favoring such structures as conduits of fluids, including magma (Rosenberg, 2004), as well as representing loci of magma generation (Leloup et al., 1999) and emplacement (Rosenberg, 2004), hence further increasing the importance of shear zones in the development of orogens and most other tectonic settings. Indeed, the absence of shear zones as magma pathways may favor deep entrapment of melts (Cavalcante et al., 2016) or their presence may function as an obstacle for flow of melts and crustal masses (Leech, 2008). Earlier studies have highlighted how deep strike-slip shear zones can account for the observed aspect of extrusion in collisional orogens (e.g., eastern Tibet and Indochina) by means of very large offsets on a network of splaying faults controlled by upper-crustal strength (Tapponnier et al., 1982). Subsequent studies on modern rates of fault slip (Daout et al., 2018) and refinements on long-term geological slip rates (Phillips et al., 2004) have favored continuous deformation in Tibet with shear zones possibly working as passive markers of mantle or upper-crustal controlled deformation (England & Molnar, 1997) and renewed interest in this topic continues to yield support to both models (Daout et al., 2018).

The Neoproterozoic West Gondwana orogen represents such an example of continental collision that involves both extruding lithospheric blocks and orogens built by thrusts, as recently outlined by Ganade de Araujo et al. (2014). In the context of such orogen the Borborema Province (BP) characterizes the extrusion part with its abundant anastomosing strike-slip shear zones connecting with the Nigerian belt and additional correlatives in west Africa (Archanjo et al., 2013), while flat-lying foliations and inverted metamorphic gradients associated with thrusts have tentatively been described as "Himalayan-type" nappes within the fault
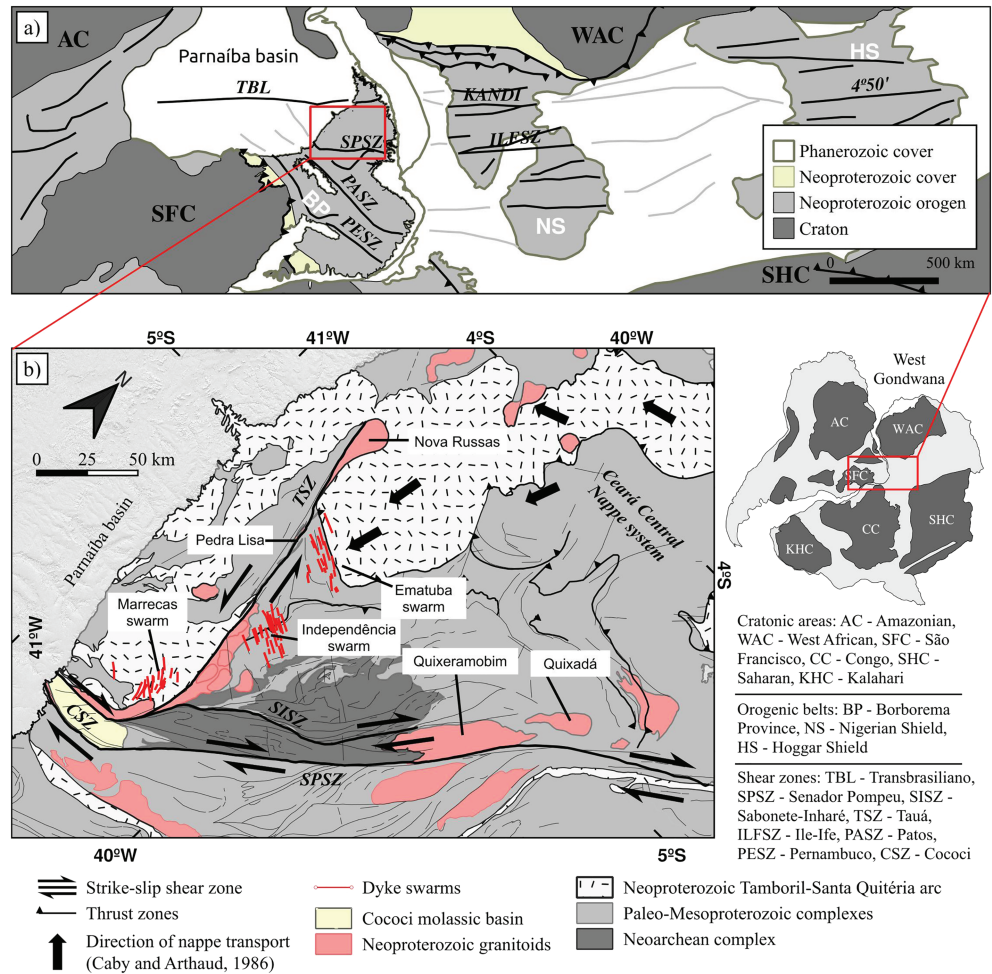
Figure 1. (a) Geological map of the central West Gondwana Orogen. (b) Geological map of the Ceará Central domain (CCD). The studied plutons are indicated by their respective names. See Figure 2 for sample locations. Note that all maps have the north rotated 45° clockwise.

bounded domains (Caby & Arthaud, 1986). This province is now exposing middle to lower crustal terranes, hence providing an opportunity to investigate how shear zone systems change character with depth and over time, how the shear zones may control exhumation during orogeny, and how thrusts and strike-slip faults are related; these are key aspects for understanding of active collisional orogens.

In the BP it is possible to constrain the full, time-integrated offset and age of shear zone activity. A common approach involves absolute dating of plutons interpreted as having formed before, during, or after shear zone activity (Archanjo et al., 2008; Oriolo et al., 2018). In this study we report the ages of plutons emplaced within or contiguous to a pair of major strike-slip shear zones, synchronous with their shear deformation, in the northwest Ceará Central domain (CCD) of BP. Magmatic deformation of the synkinematic plutons is followed by small solid-state strains, possibly indicating the important role of melt weakening and heat advection to shear zones by magma intrusion. We attempt to establish the structural-kinematic framework of these interacting strike-slip shear zones and the thrusts within the fault bounded block by also using vorticity and strain estimates. A region-wide consistent deformation field which resulted in crustal extrusion, intrusion of plutons and dykes, and, possibly, the emplacement of thrust nappes is proposed.

2. Geological Setting

The CCD is located in the NW part of the BP, which is a 400,000-km^2 orogenic terrane formed in the Neoproterozoic (Brasiliano/Pan-African orogeny) due to collision between the Congo-São Francisco and West African cratons (Figure 1). This domain is characterized by high to medium-*T* metamorphism and
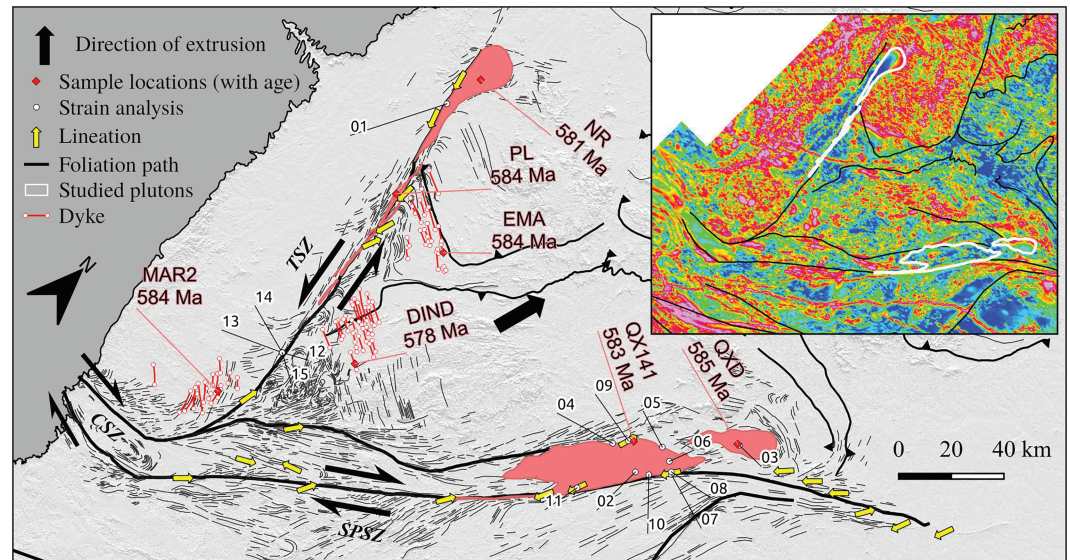
Figure 2. Structural lineaments interpreted from multispectral CBERS4 images and magnetic anomaly map (inset). Sample locations are shown with mean $^{206}Pb/^{238}U$ ages and their respective codes (QXD—Quixadá, QX141—Quixeramobim, NR—Nova Russas, PL—Pedra Lisa, EMA—Ematuba, DIND—Independência, MAR2 - Marrecas). Lineation plunges are less than 30°.

migmatisation, abundant syntectonic to late-tectonic granitoid plutons and a network of anastomosing strike-slip shear zones (Vauchez et al., 1995). In addition to a few Archean cratonic nuclei most of the basement of the BP is composed of Rhyacian to Orosirian granite-gneiss and greenstone sequences related to the Transamazonian orogeny and of Neoproterozoic orogenic belts (Costa et al., 2015). The major shear zones have been interpreted to separate different tectonic domains, the CCD being limited to the southeast by the Senador Pompeu shear zone and to the northwest by the Transbrasiliano lineament. To the west the CCD is covered by the Paleozoic Parnaíba basin and to the east by the sedimentary cover of the Atlantic coast. In a predrift reconstruction the province is correlated with Pan-African belts of western Africa, with Senador Pompeu and Transbrasiliano lineaments being connected to Ile-Ife and Kandi lineaments, respectively (Figure 1, Archanjo et al., 2013).

Within the CCD (Figure 1b) the Neoarchean Cruzeta Complex is rimmed to the northwest by accreted Rhyacian terranes (Fetter et al., 2003) which, in turn, are interleaved with Neoproterozoic metasedimentary rocks metamorphosed to varying grades (Arthaud et al., 2015). The earliest record of the Neoproterozoic Brasiliano collage starts with the Tamboril-Santa Quitéria magmatic arc in the Late Tonian and proceeds to a collisional setting through to Middle Ediacaran (Fetter et al., 2003). This arc consists mostly of migmatitic rocks intruded by syncollisional granitoids dated at circa 620 Ma but may have had its initation as early as 800 Ma (Ganade de Araujo et al., 2014); it is also believed to be the last manifestation of continental collision in the CCD, which was then followed by pervasive strike-slip tectonics. A variety of granitoid plutons and felsic dykes occur throughout the area and are thought to be syntectonic to late tectonic. These include the Nova Russas and Pedra Lisa plutons, Ematuba, Independência, and Marrecas dyke swarms and Quixeramobim and Quixadá batholiths (Figure 1). The plutons are mostly granites, monzonites, granodiorites, and tonalites, whereas the dykes are composed of porphyritic dacites to rhyolites. These dykes have not yet been found near the shear zones; thus, crosscutting relations are not directly seen.

3. The Senador Pompeu and Tauá Shear Zones

Multispectral satellite imagery and airborne magnetic survey data were used to produce maps that highlight significant structures. CBERS high-resolution images at the pancromatic band have revealed the structural grain of both shear zones and particularly of the area where the two shear zones merge. The intepretation is shown in Figure 2. Airborne magnetic survey data (made available by the Brazilian Geological Survey) were processed for the area encompassing most of the length of the shear zones. An amplitude of analytic signal filter processing applied to magnetic data reduced to the magnetic pole and with upward continuation to

500 m from ground level is shown in the inset map of Figure 2. Among other applied filters the amplitude of analytic signal was the most effective for showing deeper structures and stronger contrasts, providing additional clues to the structural lineaments map.

The deformation in the CCD is characterized by a system of southwest and south moving allochtonous units collectively known as the "Ceará Central crystalline nappes" (Caby & Arthaud, 1986) and major strike-slip faults such as the Senador Pompeu (SPSZ) and Tauá (TSZ) shear zones (Figure 2). The SPSZ is a NE trending dextral shear zone measuring ~350 km in length from its southwest intersection with the TSZ to the NE Brazilian coast. In a predrift Gondwana reconstruction, the SPSZ is roughly continuous with the Ilesha-Ifewara shear zone of southwest Nigeria (Archanjo et al., 2013; Caby & Boessé, 2001). It cuts through Archean-Paleoproterozoic basement rocks deformed at various temperatures, including local high-temperature granulite-facies mylonites dominating the northern half and amphibolite to greenschist-facies mylonites occurring along the southern half of the shear zone (Vauchez et al., 1995). Pseudotachylites and breccias occur in the southern segment. Mylonitic foliations are steeply dipping, and stretching lineations are mostly subhorizontal. Flat-lying foliations from adjoining areas are transposed by the strike-slip deformation and form upright folds close to the shear zone. Its width ranges from 1–2 km and up to 16 km to the north when it merges with the Orós-Jaguaribe shear zone. No estimates of offset exist for the SPSZ. A crustal scale vertical boundary is revealed in magnetotelluric (Padilha et al., 2017) and gravity data (Oliveira & Medeiros, 2018) beneath the SPSZ. To the northwest of the SPSZ occurs the Sabonete-Inharé shear zone (SISZ). It consists of a dextral discrete mylonite zone cutting through the Neoarchean basement. It is parallel to SPSZ and extends for ~180 km, from its junction with the Tauá shear zone to the southwest to the Quixadá batholith to the northeast where it probably splays into minor high-temperature zones and becomes indistinct. Gammaspectrometric images of the SISZ indicate that it causes only minor displacements within the basement.

The sinistral TSZ extends for ~220 km in a N10°W strike from its intersection with SPSZ to the south, to the Transbrasiliano lineament to the north. It has a thickness of ~5 km with steeply dipping foliations that are deflected in a sinistral sense on both sides of the fault, while mineral and stretching lineations are mostly horizontal. Neves (1991) has estimated an offset of 30–35 km (thus with an average shear strain of 10) from deflected NW striking structures in agreement with ~30 km offset of the tail of the *en cornue* Nova Russas pluton (see Figures 1 and 2). The shear zone cuts accross migmatites and anatexites of the Tamboril-Santa Quitéria arc (Neves, 1991) and is composed of high-temperature mylonites to cataclasites, the latter often overprinting previous ductile deformation. The core of the TSZ includes a set of anastomosing sheets of porphyritic granitoids (Pedra Lisa suite) which defines a linear magnetic low following most of the length of TSZ (inset of Figure 2), from the Nova Russas pluton southward. This magnetic low indicates a magma-laden character for the shear zone core at depth and in addition to gravity data (Oliveira & Medeiros, 2018) reveal how the TSZ causes an offset to the Tamboril-Santa Quitéria arc, juxtaposing it to the schist complex to the east. The TSZ is underlain by east dipping seismic reflectors with slightly folded geometries (Daly et al., 2014) at fairly shallow depths. In addition to that, magnetotelluric results (Padilha et al., 2017) suggest that the TSZ is a shallow structure rooted at middle-lower crustal detachments dipping east.

The SPSZ and TSZ merge to the southwest and bend into an EW strike direction. Stretching lineations of both TSZ and SPSZ plunge away from that point of convergence (i.e., lineations plunge N for TSZ and NE for SPSZ, Figure 2), whereas farther away from their junction lineations tend to plunge in the opposite direction. The EW dextral shear zone segment that forms from the intersection between TSZ and SPSZ is here termed Cococi shear zone (CSZ). This segment was reactivated at later times under a brittle pull-apart regime during which the Cococi molassic basin was formed. Thus, most of the core of the shear zone is buried, and mylonite exposures are scarce on either shoulder of the basin. Such mylonites indicate greenschist facies conditions during dextral shearing.

4. Analytical Methods

Zircons for U-Th-Pb analysis were recovered after crushing fresh hand samples (2–5 kg) and separating the different grain fractions by hydraulic, magnetic, and density methods. The zircon grains were mounted in epoxy resin together with chips of the TEMORA 1 reference zircons (Black et al., 2004). They were polished and imaged with transmitted light and. This procedure allows recognition of best grains for analysis; that is, those with no fractures, inclusions, or signs of metamictization. Analyses were focused on areas
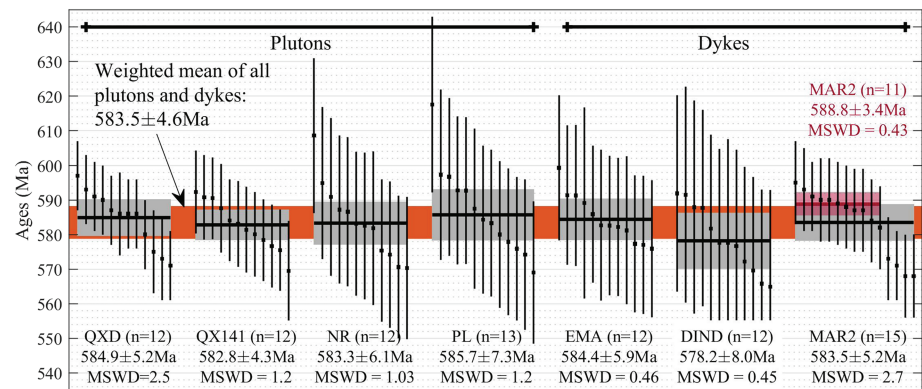
Figure 3. Weighted average $^{238}U/^{238}U$ ages for the granitoid plutons and felsic dyke swarms. Sample codes are as defined in Figure 2. Vertical lengths are analytical errors at 2σ centered at the age. Gray bars are weighted average ages with 2σ uncertainty. For cathodoluminescence images, concordia plots, and data of individual analyses see supporting information. Dark red weighted average is calculated for Marrecas sample without the four youngest ages.

of pronounced oscillatory zoning typical of primary igneous crystals. In situ analyses were conducted in SHRIMP IIe at the Geochronological Research Center of the *Universidade de São Paulo*. The isotopic data were collected in sets of five scans through the masses and the TEMORA standard measured after four unknowns (see details in Sato et al., 2014). Data reduction was performed on SQUID 2.5 and statistical assessments calculated using ISOPLOT 2.2 (Ludwig, 2009). The ages calculated are presented with errors of 2σ (95% confidence). The tabulated analysis data, concordia plots, and cathodoluminescence images of zircons are given in the supporting information. Sample locations are given in Figure 2.

5. Results
5.1. SHRIMP Ages
5.1.1. Quixadá and Quixeramobim
The Quixadá sample consists of monzodiorite rocks with alkali-feldspar and plagioclase megacrysts up to 10 cm in size in a dark green coarse-grained biotite and amphibole-rich matrix. The Quixeramobim sample consists of a porphyritic granodiorite with feldspar phenocrysts up to 6 cm in size in a coarse-grained matrix of quartz, feldspar, and biotite. Apatite, magnetite, and epidote are accessory phases in both Quixadá and Quixeramobim batholiths. Zircons from the respective granitic samples are similar with average size and aspect ratio of 135 μm and 2:1, respectively. They exhibit conspicuous magmatic oscillatory zoning. The analyses were focused on the inclusion-free oscillatory zoning domains that record crystallization age of the zircon (Figure 3).

For the Quixadá sample most of the single-grain $^{206}Pb/^{238}U$ ages (12 spots) range between 571 and 597 Ma. Three analyses not belonging to the most coherent group and with ages of circa 555 Ma (Spot 2.1; see supporting information) and circa 606 Ma (spots 8.1 and 15.1) were discarded. The remaining data set yielded a good concordia age of 585 ± 3 Ma (MSWD=0.39; see supporting information for concordia plots) and a weighted average age of 585 ± 5 Ma (MSWD=2.5, Figure 3), thus setting circa 585 Ma as an accurate estimate of age of emplacement for the Quixadá magmas.

Zircons within the Quixeramobim batholith yield a poor concordia age of 584 ± 5 Ma (MSWD = 8.4) and a weighted mean age of 583 ± 4 Ma (MSWD = 1.2, Figure 3) from the most coherent group of analyses (12 spots). Ages were calculated after removal of analyses with high U (Spot 3.1) or common ^{206}Pb (Spots 2.1 and 6.1) and ages not belonging to the most coherent group (Spots 4.1, 5.1, and 10.1).

5.1.2. Nova Russas and Pedra Lisa Plutons
Coarse-grained, porphyritic, and slightly deformed biotite-rich granodiorite samples from the Pedra Lisa suite provided zircons with pronounced oscillatory zoning. Truncated zoning indicates possible inherited xenocrystic or antecrystic cores which were not analyzed. Their average size and aspect ratios are 137 μm and 2:1, respectively. The sample from the core of Nova Russas pluton is a coarse grained, aphyric, and undeformed hornblende-biotite monzogranite having zircons much like those of Pedra Lisa with smaller grain size (130 μm) and rich in large apatite inclusions (which were also avoided during the analysis).

The ages of the analyzed Pedra Lisa zircon grains range from 569 to 617 Ma. Individual analyses have concordant $^{206}Pb/^{238}U$ and $^{207}Pb/^{235}U$ ages which are scattered over the concordia, providing a poorly defined concordia age of 587 ± 6 Ma (MSWD=8.3, 13 spots). One analysis (Spot 11.1) with an older age of 626 Ma and very low Th/U compared to other analyses was discarded. The remaining dataset forms the most coherent group with a weighted average age of 586 ± 7 Ma (MSWD=1.2) providing the best estimate of crystallization of the Pedra Lisa suite magmas.

For the Nova Russas pluton, three analyses with comparatively high values of U and ^{204}Pb, and with ages between 548 and 555 Ma, were discarded (Spots 2.1, 3.1, and 5.1). The remaining zircons form the most coherent group (12 spots) with $^{206}Pb/^{238}U$ ages varying from 570 to 608 Ma. These yield a poor concordia age of 583 ± 6 Ma (MSWD=0.0007). Thus, we take the weighted mean age of 583 ± 6 Ma (MSWD=1.03, Figure 3) as best estimate of crystallization of the Nova Russas pluton.

5.1.3. Ematuba, Independência, and Marrecas Dyke Swarms

Samples of the Ematuba, Independência, and Marrecas dykes show similar composition and texture. They are porphyritic with 0.5–1 cm large biotite, hornblende, and plagioclase phenocrysts in a trachytic to rhyolitic aphanitic groundmass. A myriad of variations to the typical texture include embayed quartz phenocrysts, large magmatic epidote, sagenitic biotite phenocrysts, rapakivi feldspar, anorthosite microenclaves, and anthophylite aggregates with biotite corona. Zircons in these rocks obtained from unaltered samples are typically euhedral with pronounced oscillatory zoning, contain a distinctly high amount of apatite inclusions of various sizes, and have an average aspect ratio of 2:1. The dated zircons from Ematuba had average size of 130 μm. The Indenpendência dyke sample had zircons with fewer inclusions and less pronounced oscillatory zoning, with average size of 122 μm. Zircons from Marrecas dykes are very homogeneous with average size of 140 μm. Analyses of all zircons were preferentially focused on well-developed zoning sites distant from inclusions and fractures. Homogeneous cores of possibly inherited origin were avoided.

Ematuba zircons forming the most coherent group (12 analyses) had $^{206}Pb/^{238}U$ ages of 575 to 599 Ma, with a poor concordia age of 586 ± 8 Ma (MSWD=11.1). Three discarded analyses (Spots 8.1, 10.1, and 13.1) were characterized by large uncertainties and were strongly discordant falling below the concordia (see supporting information). Thus, the weighted average age of 584 ± 6 Ma (MSWD=0.46) provided by the most coherent group is the best estimate for the age of the Ematuba dykes.

Analyses on 12 spots of the Independência zircons give a poor concordia age at 579 ± 8 Ma (MSWD = 0.31) and a similar weighted mean age at 578 ± 8 Ma (MSWD = 0.45, Figure 3). These were calculated after discarding four analyses with high ^{204}Pb causing large uncertainties (Spots 3.1, 4.1, 5.1, and 7.1).

Zircons from the Marrecas dykes provided the lowest uncertainties with individual ages (15 spots) ranging from 568 to 595 Ma. Two analyses (Spots 3.1 and 6.1) with significantly older $^{206}Pb/^{238}U$ ages of 627 and 625 Ma, outliers to the most coherent group, were discarded. The coherent data set yielded a good concordia age of 584 ± 3 Ma (MSWD=0.79) and an equivalent weighted average age of 584 ± 5 Ma (MSWD=2.7), which we thus take as the age of emplacement for the Marrecas dyke swarm.

5.2. Magmatic Deformation Structures and Mylonites

Several structural criteria from macroscale to microscale have been adopted to indicate the syntectonic emplacement of granitic magmas. In a regional scale the tear (*en cornue*) shape of deep-seated intrusions records syntectonic magmatism and the asymmetry of the pluton's tail has been used to define the emplacement kinematics (Romn-Berdiel et al., 1997; Rosenberg, 2004). The Nova Russas is a typical asymmetric tear-shaped pluton in agreement with the sinistral movement of the Tauá shear zone. The Quixadá batholith also has a tear-drop shape in agreement with the dextral movement of the SPSZ (Figure 4a). Romn-Berdiel et al. (1997) showed by means of analog modeling of granite emplacement in shear zones that the *en cornue* shape of plutons is formed when the feeder zone for pluton construction is located outside the shear zone core, which then deforms the pluton into a tear-drop shape. A feeder zone for the Quixadá pluton is inferred from both gravity (de Castro et al., 2002) and magnetic (magnetic high around the NW contact of the batholith, Figure 2) anomalies to be located at its NW margin.

Shape preferred orientation of feldspar phenocrysts in a granitoid where the matrix is not affected by conspicuous solid-state deformation (e.g., equant magmatic quartz) is often a reliable indicator of synmagmatic deformation. The Quixeramobim batholith bounding the SPSZ and Pedra Lisa sheet-like plutons within the TSZ is characterized by synmagmatic deformation of feldspar megacrystic granitoid facies (Figures 4b
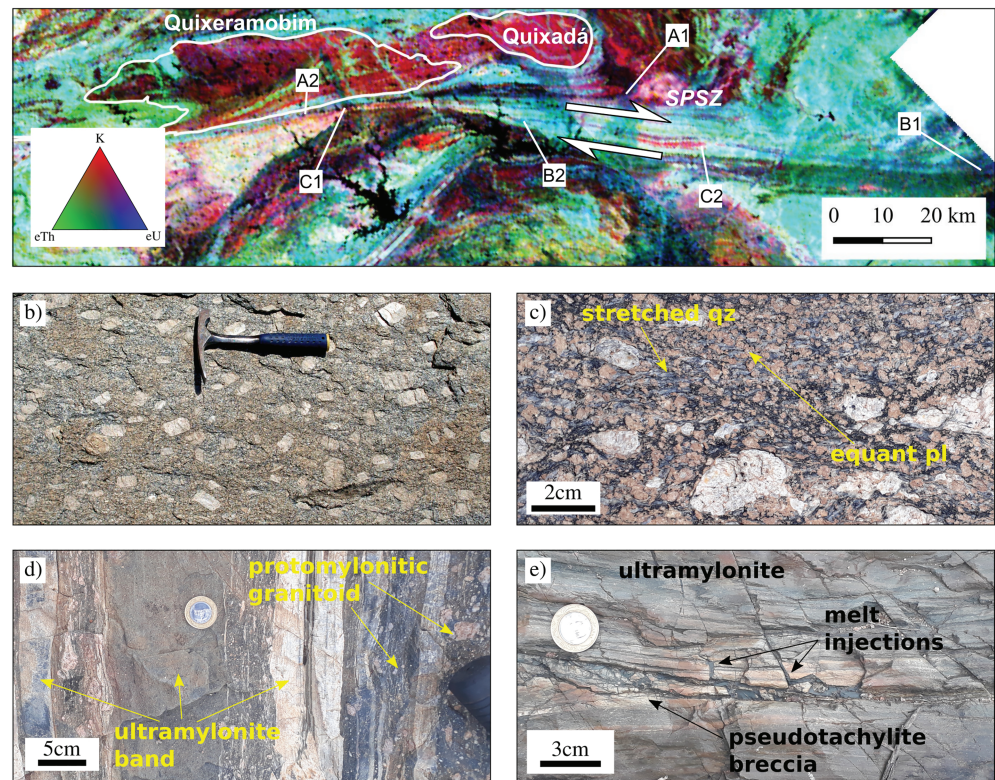
Figure 4. (a) Gamma ray spectrometry map (ternary composition) of Senador Pompeu shear zone (SPSZ). Lithological control points give offset estimates of 66, (A1–A2) 96 (B1–B2) and 68 km (C1–C2). (b) Megacrystic facies SPO of the Quixeramobim batholith (magmatic foliation is horizontal). (c) Megacrystic Quixeramobim granitoid with solid-state deformation (elongate quartz) overprinting magmatic deformation (strong SPO of equant feldspars), SPSZ. (d) SPSZ mylonite zone with banded ultramylonites, protomylonites, and lightly deformed porphyritic granites. (e) Pseudotachylite in southern segment of SPSZ. All figures have dextral shear sense.

and 5a) where a shape preferred orientation is defined by feldspar megacrysts and biotite grains in the matrix. In thin sections these fabrics show equant magmatic quartz, undeformed feldspar and biotite, and epidote-rich shear bands forming after late-magmatic plagioclase alteration (Figure 5b). Similar synmagmatic deformation of megacrystic facies occurs in the Quixadá batholith, whereas for the Nova Russas pluton, which is mostly equigranular to slightly porphyritic, magmatic deformation fabrics are less evident. In addition, mafic and megacrystic facies of the Quixeramobim batholith occurring as sheets and synmagmatic dykes are deflected toward SPSZ, as are metasedimentary wall rocks (green stripes in SE margin of the Quixeramobim batholith in gammaspectrometric image, Figure 4a). These granitoid facies with feldspar megacrysts are also characterized by SC foliations (dextral shear sense for Quixeramobim batholith and sinistral for Pedra Lisa suite), creep cavitation features, and absence of shear localizations or strong compositional layering. Magmatic deformation was progressively followed by low amounts of submagmatic and solid-state strain as shown by megacrystic granitoids of SPSZ that contain deformed quartz lenses wrapping around equant feldspar crystals (Figure 4c).

Mylonites occurring in the SPSZ close to the Quixadá-Quixeramobim complex are mostly composed of metasedimentary wall rock slivers and metagranitoids. At the northern SPSZ they are mostly high-temperature mylonites, characterized by feldspar grains with large recrystallized grain sizes (i.e., formed by subgrain rotation rather than bulging recrystallization, Martelat et al., 1999) and quartz ribbons. At the southwestern strand of SPSZ close to the tail of the Quixeramobim batholith, the metamorphic grade is middle amphibolite facies, producing subgrain rotation recrystallization of quartz to lower grain sizes and *c* axis fabrics perpendicular to the foliation, suggesting a temperature decrease toward the TSZ. The typical core of the SPSZ is characterized by decimeter-thick bands of variably deformed and mylonitized granitoids, juxtaposed with ultramylonite layers (Figure 4d). Pseudotachylites occur on the southern segments of SPSZ overprinting ultramylonites and locally associated with thin brecciated layers (Figure 4e). Lithological
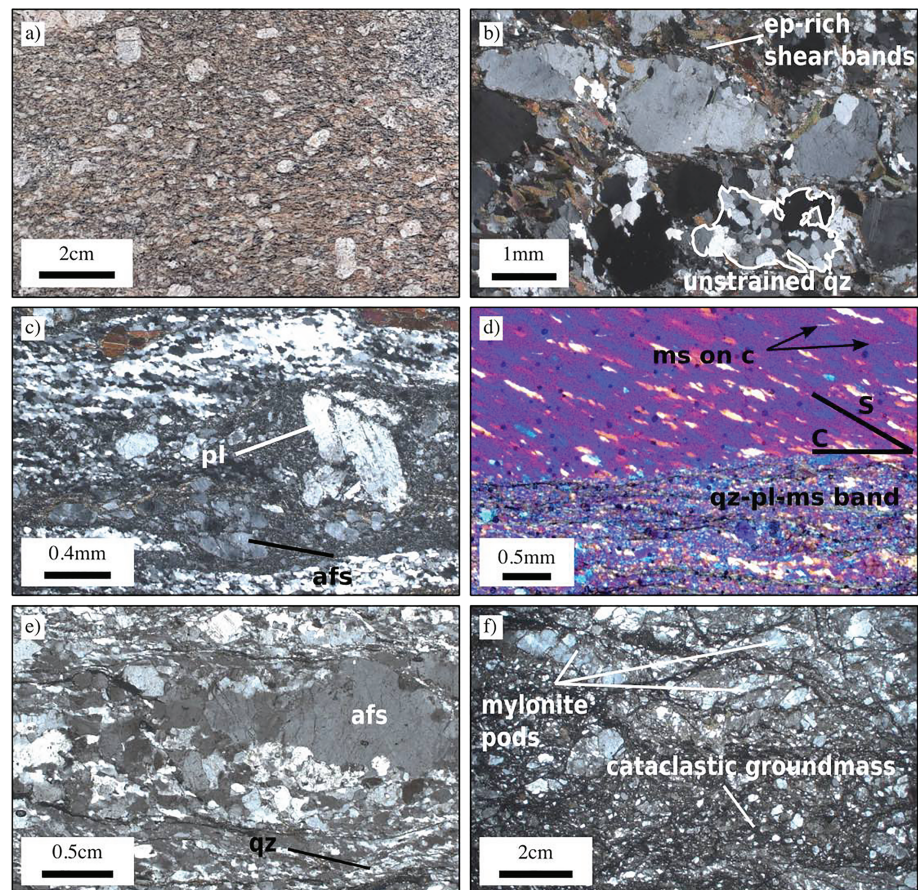
Figure 5. (a) Magmatic fabric of porphyritic facies of Pedra Lisa pluton. Foliation trace is horizontal. (b) Microstructure of Pedra-Lisa pluton deformed at submagmatic to magmatic conditions. (c) Intermediate-temperature quartz-feldspar mylonite at the fault-bounded walls of Nova Russas pluton. (d) Low-temperature S-C mylonite of southern TSZ. Note micrometer-sized muscovite laths. (e) High-temperature mylonite of middle segment of TSZ preserved from cataclastic deformation. (f) Cataclastic groundmass formed after brittle deformation overprinting high-temperature mylonites (preserved pods indicated). All figures have sinistral shear sense.

markers appreciable from gammaspectrometric composition images of SPSZ indicate an offset between 66 and 96 km (see markers on Figure 4a), which for the central segment of SPSZ (width of ~1.5 km) yields a mean shear strain of 54.

Mylonites in the TSZ are characterized by a range of deformation temperatures and conditions. Where the Nova Russas pluton intersects the shear zone at its northern segment, mineral assemblages record upper greenschist to amphibolite facies conditions with pervasive recrystallization of quartz and feldspar brittle and recrystallization-driven grain size reduction (Figure 5c). Larger strains at similar metamorphic conditions took place at the southern segment of the TSZ close to its intersection with the SPSZ (Figure 5d), where a strong compositional fabric with abundant recrystallization of feldspar and quartz is found. In the middle segment of TSZ cataclastic deformation is found to overprint plastic strain fabrics, occurring as decimeter-thick zones of brittle comminution wrapping around pods of preserved mylonites. In such pods, feldspars show large recrystallized grain sizes and mildly developed quartz ribbons occur (Figure 5e), suggesting high-temperature deformation, whereas smaller grain sizes for quartz in oblique fabrics and epidote-rich shear bands indicate an overprinting greenschist facies deformation. Thus, the cataclastic microstructures wrapping around mylonite pods (Figure 5f) indicate that the shear zone was active during progressive cooling into brittle crustal levels.

5.3. Vorticity and Kinematic Analysis

It is often challenging to find reliable structures for estimating kinematic vorticity (W_k) of flow, and each method has its own limitations (Fossen & Cavalcante, 2017; Law et al., 2004; Passchier, 1987). Megacrystic
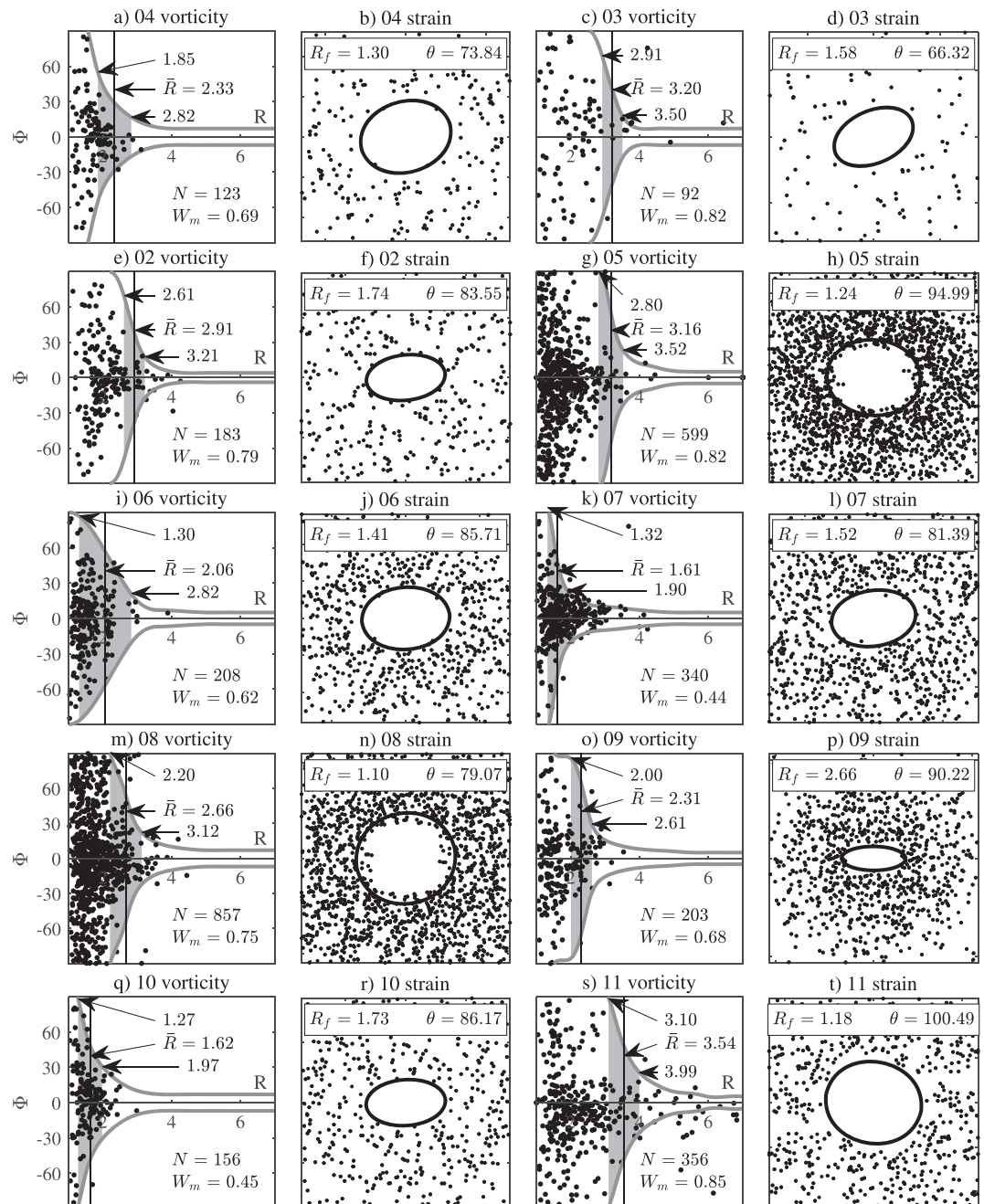
Figure 6. Kinematic vorticity and strain estimates of megacrystic facies of the Quixeramobim pluton deformed by the Senador Pompeu shear zone (SPSZ). Left charts show shape ratio of feldspar porphyroclasts (R) versus angle between feldspar long axis and the foliation plane (ϕ). $\bar{R}$ is the estimate of mean critical ratio (R_c). Right charts are strain estimates according to Fry (1979), where R_f is aspect ratio and θ is the clockwise angle between axis and foliaton pole (vertical on figure). In all cases the foliation plane is horizontal.

facies deformed in the magmatic to submagmatic state with low ensuing solid state strain such as those of Pedra Lisa suite and Quixeramobim megacrystic facies provide a good opportunity for W_k estimates by the porphyroclast method, as well as a strain estimate for the same data set by means of the Fry (1979) method. The strain recorded by these megacrystic granitoid rocks has occurred mostly in the magmatic to submagmatic state as attested by recrystallization tails in feldspar and large equant to slightly elongate quartz grains with mild undulose extinction. On those grounds we infer that the amount of solid-state strain following crystallization of the plutons has been low, although it would be difficult to assert its actual contribution
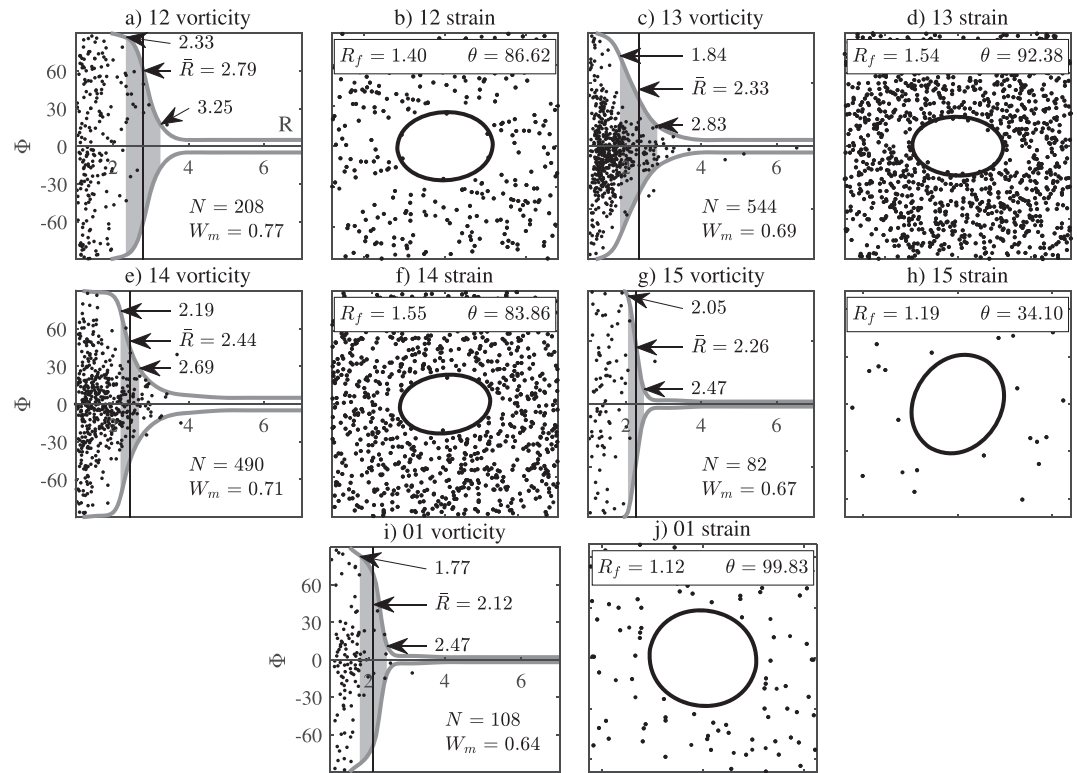
Figure 7. Kinematic vorticity and strain estimates of megacrystic facies of the Pedra Lisa and Nova Russas plutons deformed by the Tauá shear zone (TSZ). Left charts show shape ratio of feldspar porphyroclasts (R) versus angle between feldspar long axis and the foliation plane (ϕ). $\bar{R}$ is the estimate of mean critical ratio (R_c). Right charts are strain estimates according to Fry (1979), where R_f is aspect ratio and θ is the clockwise angle between axis and foliaton pole (chart north). In all cases the foliation plane is horizontal.

since strain occurs continuously through the rheological transitions of a crystallizing magma. Evidently, strain estimates from magmatic deformation structures of the granitoids represent only a snapshot of their full strain history, mostly recording only the last increment of deformation. We have attempted to estimate strain by Delauney triangulation of nearest neighbors according to a modification of the Fry (1979) method by Mulchrone (2003) using the PolyLX toolbox for Matlab (https://petrol.natur.cuni.cz/~ondro/oldweb/polylx:home; Lexa, 2003). Results are shown in Figures 6 and 7 for SPSZ and TSZ, respectively.

Sequences of photographs were taken from well-exposed surfaces of granitoids where the feldspar megacrysts were clearly visible for subsequent tracing of outlines in GNU Image Manipulation Program (Version 2.10.12). As much as possible the photos were taken of surfaces perpendicular to the magmatic foliation plane and parallel to the lineation. Images of outlined megacrysts were then processed using MATLAB (Version R2019a Update 3) for identification of best fit ellipses and their geometrical parameters (e.g., aspect ratio and orientation). Orientations of ellipses (ϕ) fit to megacrysts were plotted against axis ratio (R) in Figure 6 for megacrystic facies rocks of the Quixeramobim batholith. Kinematic vorticity is calculated according to Passchier (1987) where $W_k = (R_c^2 - 1)(R_c^2 + 1)$, and R_c is the critical aspect ratio in ϕ-R plots, which is selected as a mean value between minimum and maximum of the uncertainty region. Mean R_c values obtained for the Quixeramobim range in 1.61–3.54. W_k values for the Quixeramobim megacrystic facies fall in the range of 0.44–0.85, with an average W_k of 0.69 and standard deviation of 0.148. The percentage of pure shear relative to simple shear (Figure 8, Law et al., 2004) for that range is between 44 and 71 with a mean of 50. The strain ellipse for the same data set has a strain aspect ratio
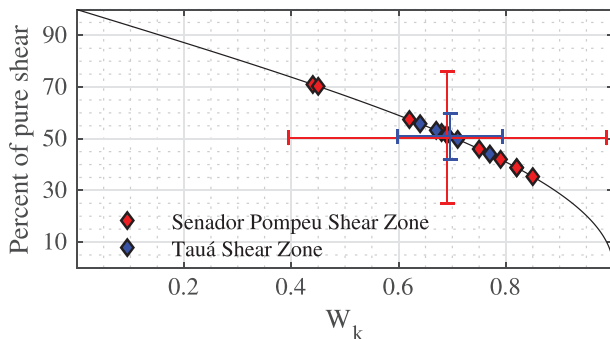

Figure 8. Relationship between percentage of pure shear relative to simple shear and kinematic vorticity (W_k). Red and blue error bars at two standard deviations centered at the means for estimates of Senador Pompeu shear zone (SPSZ) and Tauá shear zone (TSZ).

Table 1
Kinematic Vorticity (W_k), Percentage of Pure Shear (PS%), Aspect Ratio of Strain Ellipsoid (R_f), Angle of Ellipsoid Long Axis to Foliation (θ), and Thinning Estimates (a) for Megacrystic Magmas Occurring in the Senador Pompeu (SPSZ) and Tauá (TSZ) Shear Zzones

	W_k	PS%	R_f	θ	a
01 (TSZ)	0.64	56	1.12	100°	1.25
12 (TSZ)	0.77	44	1.40	87°	1.41
13 (TSZ)	0.69	52	1.54	92°	1.18
14 (TSZ)	0.71	50	1.55	84°	1.22
15 (TSZ)	0.67	53	1.19	34°	1.26
04 (SPSZ)	0.69	52	1.30	74°	1.26
03 (SPSZ)	0.82	39	1.58	66°	1.53
02 (SPSZ)	0.79	42	1.74	84°	1.37
05 (SPSZ)	0.82	39	1.24	95°	1.64
06 (SPSZ)	0.62	57	1.41	86°	1.11
07 (SPSZ)	0.44	71	1.52	81°	0.92
08 (SPSZ)	0.75	46	1.10	79°	1.46
09 (SPSZ)	0.68	52	2.66	90°	0.95
10 (SPSZ)	0.45	70	1.73	86°	0.87
11 (SPSZ)	0.85	35	1.18	100°	1.82

(X/Z of the strain ellipse) of 1.10–2.66 with a mean of 1.55. Estimated strain parameters are summarized in Table 1.

φ-R plots and strain analyses for megacrystic granitoids of the Pedra Lisa suite in southern TSZ are shown in Figure 7. R_c values ranged between ~ 2.12 and 2.79. The resulting W_k falls in the range of 0.64–0.77, with an average W_k of 0.70 and standard deviation of 0.049. Percentage of pure shear relative to simple shear is between 44 and 56 with a mean of 51 (Figure 8). The calculated strain ellipses have an aspect ratio range of 1.12–1.55 with a mean value of 1.42. Strain parameters are given in Table 1.

By combining vorticity (W_k) and shape ratio of the strain ellipsoid (R_f), it is possible to estimate the thinning (a) of the deforming layer (Festa, 2014), which for plane strain is given (Wallis et al., 1993) by

$$a = 0.5\sqrt{(1 - W_k^2)[R_f + R_f^{-1} + 2\frac{1 + W_k^2}{1 - W_k^2} + \sqrt{R_f + R_f^{-1} - 2}]}. \quad (1)$$

Often one has to use a strain gage or marker different from the structure used for vorticity estimates, which may introduce an error due to strain partitioning and heterogeneity. Thus, using the megacrystic facies SPO for both is a good opportunity for a reliable estimate of thinning, albeit such structures represent a fraction of the deformation history and thinning-thickening values may be underestimated. For the deformed Pedra Lisa suite the initial shear zone was calculated to have been 1.18 to 1.41 times thicker than the active shear zone width at the final increment of deformation (Festa, 2014), that is, a thinning of 15–30%. Estimates for the Quixeramobim batholith have a much wider range, from 1.82 to 0.87 (45% thinning to 15% thickening).

An independent gage for kinematic vorticity of the deformation affecting the TSZ is tentatively offered by the synchronous dyke swarms (Ematuba and Independência). If assumed to be pure extension fractures, these dykes have maximum extension directions at ≈ 38° to the TSZ, yielding a vorticity (W_k = (90 − 2θ), where θ is the angle between shear plane and extension direction of fractures) of ≈ 0.97 (Fossen and Cavalcante, 2017). This estimate, which is from the walls of the TSZ, is different from the one estimated within the shear zone, indicating that the pure shear component is higher within the shear zone than in the wallrocks. Additionally, magmas can be affected by strain due to some inflating component during emplacement. However, we believe that the plutons were already emplaced prior to the deformation which was recorded, and the strain related to episodic accretion of magmas was likely overprinted.

6. Discussion: A Kinematic Model for the TSZ-SPSZ Interaction
6.1. Timing of Shear Zone Activity
U-Pb isotope ratios for samples from the Marrecas dyke swarm (and to some extent the Quixadá sample) exhibit a distinct dispersion (seen from error ellipses of concordia diagrams; see supporting information) along the concordia. This dispersion from older to younger ages may well be due to the presence of an earlier population of antecrystic zircons (Leuthold et al., 2012), as it might be due to differential [206]Pb loss affecting zircons of the same population (Schoene, 2014), in which case the ages for the Marrecas dykes may indicate emplacement as early as 589 Ma if the four youngest ages (Spots 11.1, 12.1, 14.1, and 15.1) are disregarded (weighted average age plotted in magenta in Figure 3). However, compositional and textural characteristics of these younger zircons are indistinct from those of the main population and provide no reliable grounds to discard them. Moreover, these processes are unresolvable at the available precision since they lead to variations of isotope ratios that lie within the uncertainties, and since weighted average ages do not differ from concordia ages we take the former to be the most reasonable estimate of peak magmatism. The ages we obtained for the synkinematic Quixadá, Quixeramobim, Nova Russas, and Pedra Lisa plutons and for the dyke swarms emplaced away from shear zones indicate their formation at about 583.5 ± 4.6 Ma (weighted mean age). This confirms synchronous high-temperature activity of SPSZ and TSZ while the internal blocks had high brittle strength.
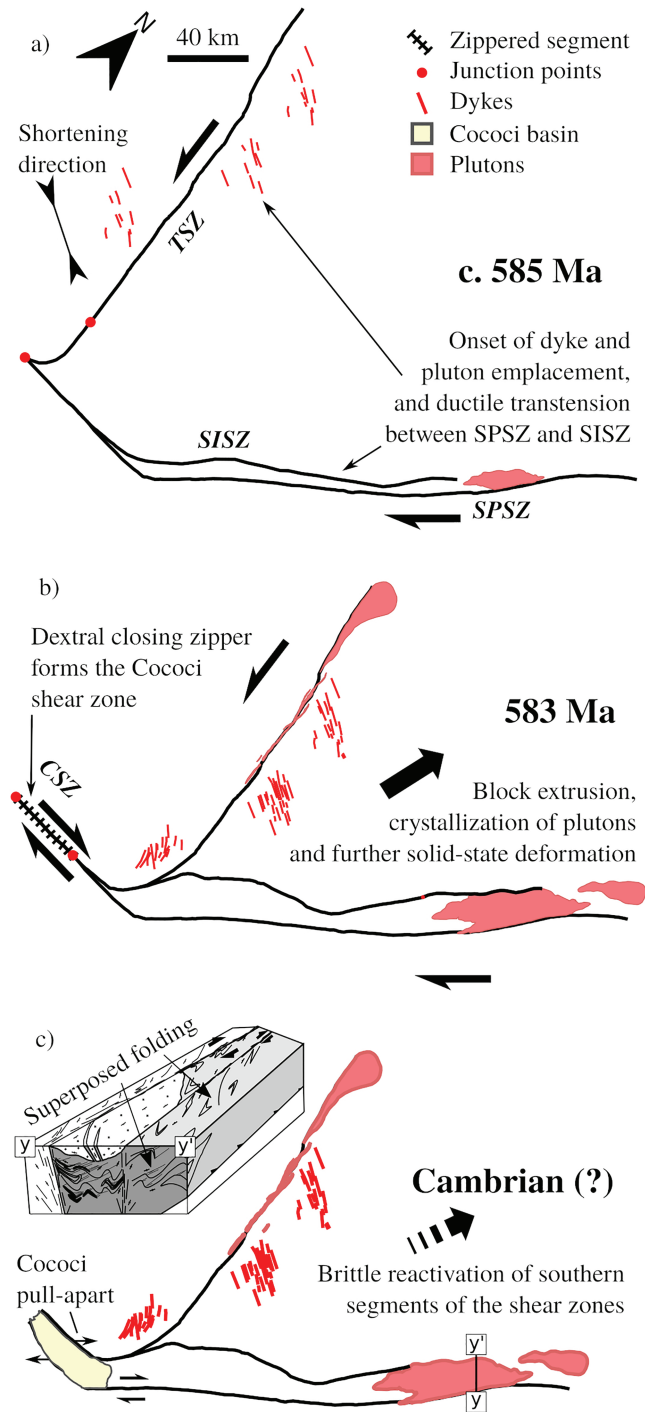
Figure 9. Model describing the geometrical framework and kinematic interactions between the Senador Pompeu (SPSZ), Tauá (TSZ), Sabonete-Inharé (SISZ), and Cococi (CSZ) shear zones in the Ceará Central Domain (CCD). See text for discussion.

6.2. Shear Zone Interaction

From the age constraints presented above we are now set to evaluate the synchronous activity of the strike-slip shear zones of the CCD. A model for this tectonic evolution is presented in Figure 9. The magnetic anomaly map (Figure 2) shows that SPSZ is bent from a NE to EW orientation after merging with TSZ to form the CSZ. Detailed observation of high-resolution CBERS4 multispectral satellite images reveals that a set of structures syntaxial with the Marrecas dykes north of the Cococi basin undergo dextral-sense deflection from

a starting orientation probably equal to that of Ematuba and Independência swarms. This is in agreement with the dextral shear of the CSZ and places a maximum shortening direction at about N60°W (assuming a tension fracture origin for the dykes) that is consistent throughout the whole domain (Figure 9a). The immediate interpretation is that of northeastward extrusion of the CCD internal block, which is interpreted to be stronger than the shear zones. At the trailing end of the block, the conjugate shear zones are zippered together forming the CSZ, which has a net dextral shear (dextral closing zipper; Passchier & Platt, 2017; Figure 9b). This requires large internal deformations in the Acaraú (west of TSZ) and Banabuiú (southeast of SPSZ) blocks. Net displacement on the zippered segment is a result of the summation of slip vectors of the interacting shear zones (Passchier & Platt, 2017). Thus, CSZ has a net dextral shear which must be a result of the SPSZ having a higher slip rate than the TSZ during their synchronous activity. Representative relations between length (L) and maximum displacements (D) for shear zones ($D = 0.017L^{1.56}$; Fossen & Cavalcante, 2017) indicate a maximum offset for TSZ of ~80 km. A sinistral deflection of structures syntaxial with the Ematuba and Independncia dyke swarms close to the TSZ has been used by Neves (1991) to estimate a total offset of 30–35 km, consistent with the minimum estimate apparent from the sheared tail of Nova Russas pluton. Therefore, we believe that synkinematic pluton emplacement occurred in late stages of shear zone activity in the CCD (Figure 9a). Also, minimum estimates of diplacement on SPSZ (Figure 4) are of about 66–96 km, thereby supporting the dextral closing zipper model for the CSZ (estimated values from length-displacements relations would be significantly higher). At this stage magmatism in shear zones was at its peak and the suite of synchronous magmas of SPSZ and TSZ was emplaced (Figure 9b). Lastly, brittle reactivation (Figure 4e) of the southern segments of TSZ and SPSZ led to a NE-SW oriented pull-apart at the CSZ on which the Cococi basin was formed, probably in the Cambrian as a precursor to the Parnaíba basin to the west (Figure 9c).

Whether these synchronous shear zones maintain the different blocks contiguous (i.e., without transverse displacements) during deformation depends on their slip rates and relative orientation. At any point it may be assumed that differential uncompensated slip rates on faults or shear zones would generate transverse deformation. A pull-apart room-making process was interpreted for the Quixadá batholith by de Castro et al. (2002) on geophysical grounds, assuming a transtensional jog with NE-SW opening. We propose that ductile transtension takes place at the SPSZ as a result of slip on the TSZ (illustrated in y-y' cross section of Figure 9c) while an uncompensated dextral shear continues on the SPSZ, therefore causing floor subsidence that facilitates emplacement of magmas to construct the Quixeramobim batholith. On a crustal scale it follows that transtension-related floor subsidence due to relative motion of shear zone-bounded terranes implies a strong spatial correlation between shear zones and plutons with emplacement favored outside fault cores rather than within (Schmidt & Paterson, 2000). The vorticities and strain ellipsoid shape ratios that were estimated in this study support this kinematic model. Because the SPO fabrics of megacrystic granitoid facies record only a snapshot of the deformation kinematics, we expect a variety of situations to emerge from interacting shear zones. The TSZ is characterized by a narrow range of W_k and thinning, with a low amount of strain being recorded at about 50% simple shear (average W_k of 0.7, Figure 8). On the other hand the SPSZ has similar average values of W_k and thinning and is distinguished by its broader range of estimated deformation parameters, including thinning and thickening, as well as percentages of simple shear varying from approximately 65% to 30%. Hence, the TSZ and SPSZ reveal a typically transpressive character of the deformation at the setting of CCD, whereas the varying character of SPSZ is related to the geometrical arrangement of the shear zone network. Expeditious Fry method strain analysis conducted by Almeida (1995) using the megacrystic facies of the Quixeramobim batholith has also shown that although most areas are consistent with the NW-SE shortening, there has been some N-S or NW-SE stretching. Further structural investigations on the Neoarchean Mombaça unit (lying southwest of the Quixeramobim pluton and bound by SPSZ and SISZ) are needed to characterize strain patterns that might hint to this hypothesis such as folding of boudinaged layers and superposed folds (inset of Figure 9c). As a first approximation, however, it may be said that structures resulting from this process may be elusive since the transtension is a transient event (or several) in a dominantly transpressive setting.

6.3. Tectonic Implications

The intrusion of dyke swarms around 584 Ma in the central part of CCD (Ematuba and Independência) and to the west of TSZ (Marrecas swarm) at midcrustal depths (c. 4.5–5.5 kbar, Nogueira, 2004) suggests a high strength of the fault-bounded blocks as compared to the plastically deforming shear zones. Considering that the SPSZ and TSZ are both abundantly permeated by magmas during their activity, with granite sheets

occurring along most of their length (Figures 2 and 4c), the role of melt weakening (Hollister & Crawford, 1986) must have been substantial. Due to their low viscosity, magmas can localize a significant amount of strain in short periods (Davidson et al., 1992; Tommasi et al., 1994). Neves et al. (1996) has propposed that the weakening induced by the presence of magma in the TSZ is the enabling factor for shear zone nucleation. Various geophysical and geological evidence indicate that the SPSZ (Padilha et al., 2017) is a preexisting (relative to late Brasiliano strike-slip deformation) crustal discontinuity in the Borborema. However, it is also affected by shear zone-concordant granite sheets, some which display only weak solid-state deformation features, possibly as a result of shear zone arrest after full magma crystallization, as described by Tommasi et al. (1994).

The development of this shear zone pair and extrusion of the internal block of the CCD is currently believed to shortly succeed the continental collision that followed long-lived arc magmatism (Ganade de Araujo et al., 2014). According to Caby and Arthaud (1986), the formation of the Ceará Central nappe system (Figure 1) would be synchronous with such an extrusion tectonics which, in turn, would place the Tamboril-Santa Quitéria arc as an allochtonous unit over the Rhyacian basement. The initial hypothesis of Caby and Arthaud (1986) about the existence of large nappes transported to SSW over long distances required the SPSZ and TSZ to act as lateral ramps, which would imply an opposite sense of shear. Geophysical evidence that the TSZ is a relatively shallow structure in the present day crust possibly indicates that it merges with a middle-lower crustal detachment. Such deeper detachment structures are likely synchronous with the development of the CCD nappes and may be related to their formation by the extrusion of the internal block. Caby and Boessé (2001) have also outlined nappe-like structures in the Nigerian belt next to the Ifewara-Ilesha shear zone, with NE-plunging stretching lineations and top to the NE (i.e., extensional) movement. Additional investigations of both provinces, however, are necessary to set the chronology and kinematic compatibility between deep-seated nappe structures and lateral strike-slip shear zones.

7. Conclusions

Interpreting the kinematic, rheological, and geochronological characteristics of interacting shear zones in the middle crust is necessary to understand the evolution of shear zone networks. In this work we have demonstrated how a zippered shear zone model applies to large-scale shearing and extrusion of crustal blocks. This approach is also essential for the understanding of processes of continental collision and orogen exhumation. Specifically, constraining timing of fault activity and their strain kinematics hint into processes ranging from pluton emplacement to transport of crustal blocks. By applying in situ U-Pb dating to dykes and synkinematic plutons of the Senador Pompeu and Tauá shear zones, we determined their synchronous activity at 583.5±4.6. Rheological heterogeneities at this level are marked by synkinematic plutons that cause melt weakening, enhanced viscous flow and later crustal welding, while felsic dyke swarms are emplaced in brittle extensional fractures. Furthermore, the arrangement of the Senador Pompeu and Tauá shear zones has formed a dextral closing zipper (CSZ) trailing the extrusion of the strong confined crustal block to the east. Such a framework agrees with the wider range of vorticity and thinning estimates recorded in the high-temperature Senador Pompeu dextral shear zone, which are thought to result from varying offset rates of the interacting shear zones and could serve as a local transtension mechanism allowing emplacement of the Quixeramobim batholith. The postcollisional deformation of the northwest part of the Borborema Province is consistent therefore with lateral escape to the north of the CCD, pluton emplacement along a conjugate set of a bulk transpressive shear system, and, in the intervening stiffer crustal fragments, brittle fracturing and emplacement of dykes.

References

Almeida, A. R. (1995). Petrologia e aspectos tectônicos do complexo granítico Quixadá-Quixeramobim, CE (PhD), Universidade de São Paulo, São Paulo.

Archanjo, C. J., Hollanda, M. H. B., Rodrigues, S. W., Neves, B. B., & Armstrong, R. (2008). Fabrics of pre- and syntectonic granite plutons and chronology of shear zones in the Eastern Borborema Province, NE. *Journal of Structural Geology*, *30*(3), 310–326. https://doi.org/10.1016/j.jsg.2007.11.011

Archanjo, C. J., Viegas, L. G., Hollanda, M. H. B., Souza, L. C., & Liu, D. (2013). Timing of the HT/LP transpression in the Neoproterozoic Seridó Belt (Borborema Province, Brazil): Constraints from UPb (SHRIMP) geochronology and implications for the connections between NE Brazil and West Africa. *Gondwana Research*, *23*(2), 701–714. https://doi.org/10.1016/j.gr.2012.05.005

Arthaud, M., Fuck, R., Dantas, E., Santos, T., Caby, R., & Armstrong, R. (2015). The Neoproterozoic Ceará Group, Ceará Central domain, NE Brazil: Depositional age and provenance of detrital material. New insights from UPb and SmNd geochronology. *Journal of South American Earth Sciences*, *58*, 223–237. https://doi.org/10.1016/j.jsames.2014.09.007

Black, L. P., Kamo, S. L., Allen, C. M., Davis, D. W., Aleinikoff, J. N., Valley, J. W., et al. (2004). Improved ^{206}Pb/^{238}U microprobe geochronology by the monitoring of a trace-element-related matrix effect: SHRIMP, IDTIMS, ELAICPMS and oxygen isotope documentation for a series of zircon standards. *Chemical Geology*, *205*(1-2), 115–140. https://doi.org/10.1016/j.chemgeo.2004.01.003

Caby, R., & Arthaud, M. (1986). Major Precambrian nappes of the Brazilian belt, Ceará, northeast Brazil. *Geology*, *14*(10), 871. https://doi.org/10.1130/0091-7613 (1986)14<871:MPNOTB>2.0.CO;2

Caby, R., & Boessé, J. (2001). Pan-African nappe system in southwest Nigeria: The Ife-Ilesha schist belt. *Journal of African Earth Sciences*, *33*(2), 211–225. https://doi.org/10.1016/S0899-5362(01)80060-9

Cavalcante, G. C. G., Viegas, G., Archanjo, C. J., & da Silva, M. E. (2016). The influence of partial melting and melt migration on the rheology of the continental crust. *Journal of Geodynamics*, *101*, 186–199. https://doi.org/10.1016/j.jog.2016.06.002

Costa, F. G. d., Palheta, E. S. d. M., Rodrigues, J. B., Gomes, I. P., & Vasconcelos, A. M. (2015). Geochemistry and UPb zircon ages of plutonic rocks from the Algodes granite-greenstone terrane, Troia Massif, northern Borborema Province, Brazil: Implications for Paleoproterozoic subduction-accretion processes. *Journal of South American Earth Sciences*, *59*, 45–68. https://doi.org/10.1016/j.jsames.2015.01.007

Daly, M. C., Andrade, V., Barousse, C. A., Costa, R., McDowell, K., Piggott, N., & Poole, A. J. (2014). Brasiliano crustal structure and the tectonic setting of the Parnaíba basin of NE Brazil: Results of a deep seismic reflection profile: Crustal structure of the Parnaíba basin. *Tectonics*, *33*, 2102–2120. https://doi.org/10.1002/2014TC003632

Daout, S., Doin, M. P., Peltzer, G., Lasserre, C., Socquet, A., Volat, M., & Sudhaus, H. (2018). Strain partitioning and present-day fault kinematics in NW Tibet from Envisat SAR interferometry. *Journal of Geophysical Research: Solid Earth*, *123*, 2462–2483. https://doi.org/10.1002/2017JB015020

Davidson, C., Hollister, S., & Schmid, S. (1992). Role of melt in the formation of a deep-crustal compressive shear zone: The MaClaren Glacier Metamorphic Belt, south central Alaska. *Tectonics*, *11*(2), 348–359. https://doi.org/10.1029/91TC02907

de Castro, D. L., Branco, R. M. G. C., Martins, G., & de Castro, N. A. (2002). Radiometric, magnetic, and gravity study of the Quixadá batholith, central Ceará domain (NE Brazil): Evidence for Pan-African/Brasiliano extension-controlled emplacement. *Journal of South American Earth Sciences*, *15*(5), 543–551. https://doi.org/10.1016/S0895-9811(02)00082-2

England, P., & Molnar, P. (1997). Active deformation of Asia: From kinematics to dynamics. *Science*, *278*(5338), 647–650. https://doi.org/10.1126/science.278.5338.647

Festa, V. (2014). The amount of pure shear and thinning in the Hercynian continental lower crust exposed in the Serre Massif (Calabria, southern Italy): An application of the vorticity analysis to quartz c-axis fabrics. *Italian Journal of Geosciences*, *133*(2), 214–222. https://doi.org/10.3301/IJG.2014.03

Fetter, A. H., Saraiva dos Santos, T. J., Van Schmus, W. R., Hackspacher, P. C., Bley de Brito Neves, B., Arthaud, M. H., Nogueira Neto, J. A., & Wernick, E. (2003). Evidence for Neoproterozoic continental arc magmatism in the Santa Quitéria Batholith of Ceará State, NW Borborema Province, NE Brazil: Implications for the assembly of West Gondwana. *Gondwana Research*, *6*(2), 265–273. https://doi.org/10.1016/S1342-937X(05)70975-8

Fossen, H., & Cavalcante, G. C. G. (2017). Shear zones. A review. *Earth-Science Reviews*, *171*, 434–455. https://doi.org/10.1016/j.earscirev.2017.05.002

Fry, N. (1979). Random point distributions and strain measurement in rocks. *Tectonophysics*, *60*(1-2), 89–105. https://doi.org/10.1016/0040-1951(79)90135-5

Ganade de Araujo, C. E., Cordani, U. G., Weinberg, R. F., Basei, M. A., Armstrong, R., & Sato, K. (2014). Tracing Neoproterozoic subduction in the Borborema Province (NE-Brazil): Clues from U-Pb geochronology and Sr-Nd-Hf-O isotopes on granitoids and migmatites. *Lithos*, *202-203*, 167–189. https://doi.org/10.1016/j.lithos.2014.05.015

Hollister, L. S., & Crawford, M. L. (1986). Melt-enhanced deformation: A major tectonic process. *Geology*, *14*(7), 558. https://doi.org/10.1130/0091-7613(1986)14<558:MDAMTP>2.0.CO;2

Law, R. D., Searle, M. P., & Simpson, R. L. (2004). Strain, deformation temperatures and vorticity of flow at the top of the Greater Himalayan Slab, Everest Massif, Tibet. *Journal of the Geological Society*, *161*(2), 305–320. https://doi.org/10.1144/0016-764903-047

Leech, M. (2008). Does the Karakoram fault interrupt mid-crustal channel flow in the western Himalaya? *Earth and Planetary Science Letters*, *276*(3-4), 314–322. https://doi.org/10.1016/j.epsl.2008.10.006

Leloup, P. H., Ricard, Y., Battaglia, J., & Lacassin, R. (1999). Shear heating in continental strike-slip shear zones: Model and field examples. *Geophysical Journal International*, *136*(1), 19–40. https://doi.org/10.1046/j.1365-246X.1999.00683.x

Leuthold, J., Mntener, O., Baumgartner, L. P., Putlitz, B., Ovtcharova, M., & Schaltegger, U. (2012). Time resolved construction of a bimodal laccolith (Torres del Paine, Patagonia). *Earth and Planetary Science Letters*, *325-326*, 85–92. https://doi.org/10.1016/j.epsl.2012.01.032

Lexa, O. (2003). Numerical approaches in structural and microstructural analyses (PhD), Charles University, Prague, Czech Republic.

Ludwig, K. R. (2009). *SQUID 2. A user's manual*. Berkeley: Berkeley Geochronology Center.

Martelat, J. E., Schulmann, K., Lardeaux, J. M., Nicollet, C., & Cardon, H. (1999). Granulite microfabrics and deformation mechanisms in southern Madagascar. *Journal of Structural Geology*, *21*(6), 671–687. https://doi.org/10.1016/S0191-8141(99)00052-8

Mulchrone, K. F. (2003). Application of Delaunay triangulation to the nearest neighbour method of strain analysis. *Journal of Structural Geology*, *25*(5), 689–702. https://doi.org/10.1016/S0191-8141(02)00067-6

Neves, S. (1991). A Zona de Cisalhamento Tauá, Ceará: Sentido e estimativa de do deslocamento, evolução estrutural e granitogênese associada. *Revista Brasileira de Geociências*, *2*(21), 161–173.

Neves, S., Vauchez, A., & Archanjo, C. (1996). Shear zone-controlled magma emplacement or magma-assisted nucleation of shear zones? Insights from northeast Brazil. *Tectonophysics*, *262*(1-4), 349–354. https://doi.org/10.1016/0040-1951(96)00007-8

Nogueira, J. (2004). *Estrutura, Geocronologia e Alojamento dos Batólitos de Quixadá, Quixeramobim e Senador Pompeu- Ceará Central*. Rio Claro, SP, Universidade Estadual Paulista.

Oliveira, R. G., & Medeiros, W. E. (2018). Deep crustal framework of the Borborema Province, NE Brazil, derived from gravity and magnetic data. *Precambrian Research*, *315*, 45–65. https://doi.org/10.1016/j.precamres.2018.07.004

Oriolo, S., Wemmer, K., Oyhantabal, P., Fossen, H., Schulz, B., & Siegesmund, S. (2018). Geochronology of shear zones. A review. *Earth-Science Reviews*, *185*, 665–683. https://doi.org/10.1016/j.earscirev.2018.07.007

Padilha, A. L., Vitorello, I., Pádua, M. B., & Fuck, R. A. (2017). Cryptic signatures of Neoproterozoic accretionary events in northeast Brazil imaged by magnetotellurics: Implications for the assembly of West Gondwana. *Tectonophysics*, *699*, 164–177. https://doi.org/10.1016/j.tecto.2017.01.022

Passchier, C. W. (1987). Stable positions of rigid objects in non-coaxial flowma study in vorticity analysis. *Journal of Structural Geology*, *9*(5/6), 679–690.

Passchier, C. W., & Platt, J. P. (2017). Shear zone junctions: Of zippers and freeways. *Journal of Structural Geology*, *95*, 188–202. https://doi.org/10.1016/j.jsg.2016.10.010

Phillips, R. J., Parrish, R. R., & Searle, M. P. (2004). Age constraints on ductile deformation and long-term slip rates along the Karakoram fault zone, Ladakh. *Earth and Planetary Science Letters*, *226*(3-4), 305–319. https://doi.org/10.1016/j.epsl.2004.07.037

Román-Berdiel, T., Gapais, D., & Brun, J. P. (1997). Granite intrusion along strike-slip zones in experiment and nature. *American Journal of Science*, *297*(6), 651–678. https://doi.org/10.2475/ajs.297.6.651

Rosenberg, C. L. (2004). Shear zones and magma ascent: A model based on a review of the Tertiary magmatism in the Alps. *Tectonics*, *23*, TC3002. https://doi.org/10.1029/2003TC001526

Sato, K., Tassinari, C. C. G., Basei, M. A. S., Siga Júnior, O., Onoe, A. T., & Souza, M. D. d. (2014). Sensitive High Resolution Ion Microprobe (SHRIMP IIe/MC) of the Institute of Geosciences of the University of São Paulo, Brazil: Analytical method and first results. *Geologia USP, Série Científica*, *14*(3), 3–18. https://doi.org/10.5327/Z1519-874X201400030001

Schmidt, K. L., & Paterson, S. R. (2000). Analyses fail to find coupling between deformation and magmatism. *Eos, Transactions American Geophysical Union*, *81*(18), 197–203.

Schoene, B. (2014). U-Th-Pb geochronology, *Treatise on geochemistry* (pp. 341–378). Amsterdam: Elsevier. https://doi.org/10.1016/B978-0-08-095975-7.00310-7

Tapponnier, P., Peltzer, G., Le Dain, A. Y., Armijo, R., & Cobbold, P. (1982). Propagating extrusion tectonics in Asia: New insights from simple experiments with plasticine. *Geology*, *10*(12), 611. https://doi.org/10.1130/0091-7613 (1982)10<611:PETIAN>2.0.CO;2

Tommasi, A., Vauchez, A., Fernandes, L., & Porcher, C. (1994). Magma-assisted strain localization in an orogen-parallel transcurrent shear zone of southern Brazil. *Tectonics*, *13*(2), 421–437. https://doi.org/10.1029/93TC03319

Vauchez, A., Neves, S., Caby, R., Corsini, M., Egydio-Silva, M., Arthaud, M., & Amaro, V. (1995). The Borborema shear zone system, NE Brazil. *Journal of South American Earth Sciences*, *8*(3-4), 247–266. https://doi.org/10.1016/0895-9811(95)00012-5

Wallis, S. R., Platt, J. P., & Knott, S. D. (1993). Recognition of syn-convergence extension in accretionary wedges with examples from the Calabrian Arc and the Eastern Alps. *American Journal of Science*, *293*(5), 463–494. https://doi.org/10.2475/ajs.293.5.463

Yakovlev, P. V., & Clark, M. K. (2014). Conservation and redistribution of crust during the Indo-Asian collision: Mass balance of the Indo-Asian orogen. *Tectonics*, *33*, 1016–1027. https://doi.org/10.1002/2013TC003469